Clinical Cancer Research

Effective Delivery of a Microtubule Polymerization Inhibitor Synergizes with Standard Regimens in Models of Pancreatic Ductal Adenocarcinoma

Jaime A. Eberle-Singh[1,2], Irina Sagalovskiy[1,2], H. Carlo Maurer[1,2], Stephen A. Sastra[1,2], Carmine F. Palermo[1,2], Amanda R. Decker[1,2], Min Jung Kim[3], Josephine Sheedy[3], Anna Mollin[3], Liangxian Cao[3], Jianhua Hu[2,4], Arthur Branstrom[3], Marla Weetall[3], and Kenneth P. Olive[1,2]

Abstract

Purpose: Pancreatic ductal adenocarcinoma (PDA) is a deadly cancer that is broadly chemoresistant, due in part to biophysical properties of tumor stroma, which serves as a barrier to drug delivery for most classical chemotherapeutic drugs. The goal of this work is to evaluate the preclinical efficacy and mechanisms of PTC596, a novel agent with potent anticancer properties *in vitro* and desirable pharmacologic properties *in vivo*.

Experimental Design: We assessed the pharmacology, mechanism, and preclinical efficacy of PTC596 in combination with standards of care, using multiple preclinical models of PDA.

Results: We found that PTC596 has pharmacologic properties that overcome the barrier to drug delivery in PDA, including a long circulating half-life, lack of P-glycoprotein substrate activity, and high systemic tolerability. We also found that PTC596 combined synergistically with standard clinical regimens to improve efficacy in multiple model systems, including the chemoresistant genetically engineered "KPC" model of PDA. Through mechanistic studies, we learned that PTC596 functions as a direct microtubule polymerization inhibitor, yet a prior clinical trial found that it lacks peripheral neurotoxicity, in contrast to other such agents. Strikingly, we found that PTC596 synergized with the standard clinical backbone regimen gemcitabine/nab-paclitaxel, yielding potent, durable regressions in a PDX model. Moreover, similar efficacy was achieved in combination with nab-paclitaxel alone, highlighting a specific synergistic interaction between two different microtubule-targeted agents in the setting of pancreatic ductal adenocarcinoma.

Conclusions: These data demonstrate clear rationale for the development of PTC596 in combination with standard-of-care chemotherapy for PDA.

Introduction

An estimated 56,770 Americans will be diagnosed with pancreatic cancer in 2019 and this figure is predicted to rise over the next decade (1, 2). Pancreatic ductal adenocarcinoma accounts for approximately 93% of pancreatic tumors but, despite some measurable progress in recent years, it remains a largely intractable cancer, with a 5-year survival rate of 8.7% (3). Among the most remarkable features of PDA is its broad primary resistance to chemotherapy, which is conferred at least, in part, by properties of the tumor stroma that limit drug delivery (4, 5). We previously elucidated this concept using the *Kras*$^{LSL.G12D/+}$; *Tp53*$^{LSL.R172H/+}$; *PdxCre*$^{tg/+}$ (KPC) mouse (6), a well-validated genetically engineered model of PDA that recapitulates many of the features of human pancreatic cancer, including stromal desmoplasia and chemoresistance (4). Thus, the KPC mouse serves as a highly stringent system in which to test the preclinical efficacy of novel agents for PDA.

On the basis of our earlier findings, we proposed that drug development efforts for PDA should focus on agents with a long half-life and a large therapeutic index (the range of concentrations between efficacy and toxicity) as a means of improving drug exposure (4). Unfortunately, most traditional cytotoxic agents are rapidly cleared from circulation, are acutely toxic to normal proliferating tissues, are quickly metabolized, or are actively exported from tumor cells. An informative counterexample is nab-paclitaxel (Abraxane, Celgene), an albumin-bound form of the microtubule-stabilizing agent paclitaxel that is FDA approved in combination with gemcitabine (a deoxycytidine analogue) for patients with metastatic PDA (7). Nab-paclitaxel has a terminal half-life of 27 hours in circulation and is less toxic than unmodified paclitaxel (8). The clinical success of the

[1]Division of Digestive and Liver Diseases, Department of Medicine, Columbia University Medical Center, New York, New York. [2]Herbert Irving Comprehensive Cancer Center, Columbia University Medical Center, New York, New York. [3]PTC Therapeutics, South Plainfield, New Jersey. [4]Department of Biostatistics, Columbia University Medical Center, New York, New York.

Note: Supplementary data for this article are available at Clinical Cancer Research Online (http://clincancerres.aacrjournals.org/).

Transcriptomics data: Transcriptomic data generated in this work may be accessed via the GEO repository using the following confidential reviewer token: ID: GSE118441 (token: krmbkmqebpajnuh).

Corresponding Author: Kenneth P. Olive, Columbia University Medical Center, 1130 Saint Nicholas Ave., ICRC 216, New York, NY 10032. Phone: 212-851-4678; Fax: 212-851-4660; E-mail: kenolive@columbia.edu

Clin Cancer Res 2019;25:5548–60

doi: 10.1158/1078-0432.CCR-18-3281

Translational Relevance

Pancreatic ductal adenocarcinoma (PDA) is responsible for more than 44,000 deaths per year in the United States. It is characterized by broad primary chemoresistance conferred, in part, by biophysical properties of the tumor stroma that interfere with drug delivery. Here we present and characterize PTC596, a novel microtubule polymerization inhibitor that demonstrates unusually promising pharmacologic properties that bypass this barrier to drug delivery. Using multiple preclinical models, we demonstrate effective delivery of PTC596 to pancreatic tumor tissues, excellent tolerability, and significant preclinical efficacy in combination with standard therapies. In particular, PTC596 synergized potently with the nab-paclitaxel, a microtubule-stabilizing agent used in combination with gemcitabine, providing strong evidence for combining these two distinct classes of microtubule-targeted agents in patients with PDA.

gemcitabine/nab-paclitaxel combination (which now serves as a standard backbone regimen for new clinical trials) helped to demonstrate the importance of pharmacology in pancreatic cancer drug development.

In the course of our work, we evaluated PTC596 (PTC Therapeutics, Supplementary Fig. S1), a small-molecule anticancer agent originally identified for its selective activity in cell lines with high levels of BMI1 protein (9). We found that PTC596 potently induces mitotic arrest and apoptosis in multiple PDA cell lines. More unusual, we found that PTC596 has attractive pharmacologic properties, including a long circulating half-life, lack of P-glycoprotein (P-gp) substrate activity, and effective biodistribution into autochthonous pancreatic tumors. Through a combination of transcriptomic, cellular, and biochemical studies, we determined that the mechanism of action of PTC596 is through direct inhibition of tubulin polymerization, although, in contradistinction to other microtubule-targeted agents (MTA), PTC596 is very well tolerated *in vivo*. Critically, intervention studies in multiple preclinical models, including the genetically engineered KPC model, a cell line–based xenograft, and a patient-derived xenograft, demonstrated potent activity of PTC596 in combination with common backbone regimens for PDA. In particular, combining PTC596 with gemcitabine/nab-paclitaxel, or even just with nab-paclitaxel alone, produced frank, durable regressions in a patient-derived xenograft model of PDA, revealing a synergistic interaction between two distinct MTAs, each possessing strong pharmacologic properties.

Materials and Methods

Additional details are presented in Supplementary Materials for all experiments.

Animal studies

All animal studies were carried out in accordance with approved Institutional Care and Use Committee protocols for Columbia University Medical Center (AC-AAAQ-1415), PTC Therapeutics, or Champions Oncology (PDX Model).

Cell lines, cell culture, and viability assays

Authenticated human cell lines were purchased from ATCC, utilized within 30 cumulative passages of initial purchase. Murine KPC lines were generated previously by KPO and used within 30 cumulative passages. J1002 cells were generated by JAE from KPFBR mice and used within 15 cumulative passages. All cell lines consistently tested negative for *Mycoplasma* throughout the period of experimentation using the MycoAlert Mycoplasma Detection Kit (Lonza). Cells were cultured in DMEM + 10% FBS with penicillin/streptomycin. Proliferation and dose–response curves were performed in 96-well plates, with viability measured by AlamarBlue (Bio-Rad) according to standard protocols. All assays were carried out in at least triplicate with 4–8 technical replicates per treatment group, per experiment. Colony formation assays were performed according to standard protocols, with 3,000 cells per 6-well for murine cells and 5,000 cells per 6 wells for human cells, in triplicate.

Flow cytometry

For cell-cycle analysis, log-growth phase cells were treated with agents as indicated, harvested, fixed in cold 70% ethanol, resuspended in PBS + 2% FBS + 3 μmol/L DAPI or 0.25 μg 7-AAD, and analyzed using a MACSQuant Analyzer 10 (Miltenyi Biotec) or BD LSRII. Data were analyzed using FlowJo software. For intracellular proteins, experimental conditions were similar, but cells were fixed/permeabilized using the eBioscience Foxp3/Transcription Factor Staining Buffer Set (Thermo Fisher Scientific, 00-5523-00), blocked with Fc Block (BD Biosciences, 564220), and stained with anti-PH3 (BioLegend, 650805), analyzed on a BD Fortessa, and analyzed by FlowJo. Active caspase-3 was performed according to manufacturer's instructions (Abcam, ab65613).

Western blotting

Western blotting was performed according to standard procedures using the following antibodies: Bmi1 (Cell Signaling Technology #5856, 1:1,000), Vinculin (Cell Signaling Technology #4650S, 1:1,000), β-tubulin (Cell Signaling Technology #2146S, 1:1,000), and anti-rabbit IgG, HRP-linked antibody (Cell Signaling Technology, #7074, 1:5,000).

P-glycoprotein substrate activity experiment

MDCKII-mdr1 and MDCKII-wt cells were purchased from the Netherlands Cancer Institute (NKI-AVL, Amsterdam, the Netherlands). Cells were cultivated in DMEM + FBS + 1% penicillin/streptomycin, and used between passages 3 and 9. Cells were plated for 4 hours, treated as indicated, and viability measured using Cell Titer-Glo (Promega).

RNA sequencing

Illumina Tur-Seq RNA libraries were prepared from poly-A enriched mRNA and sequenced on an Illumina HiSeq 4,000 to 30 million 100-bp single reads. Reads were mapped to (NCBI/build 37.2) using the STAR aligner (version 2.4.2; ref. 10) and were quantified at the gene level using the *summarizeOverlaps* function from the R package "GenomicAlignments" (11) with information on gene annotations from the R package "TxDb.Hsapiens.UCSC.hg19.knownGene" (12). RNA-seq data were deposited to GEO (ID: GSE118441).

Expression analysis

Differential gene expression was performed using the *voom-limma* framework (13). Single-sample GSEA: gene set variation analysis was performed in R according to default parameters (14).

Cell-free tubulin polymerization assay

Assay was performed using the fluorescence-based tubulin polymerization assay kit from Cytoskeleton (#BK011P), according to instructions. Polymerization rates (fluorescence units/minute) were determined by measuring the maximal slope (by linear regression) of the linear portion of the growth phase of the polymerization curve.

Analysis of free tubulin content

Free versus polymerized tubulin was measured using the Microtubule/Tubulin In Vivo Assay Biochem Kit (Cytoskeleton, #BK038).

Immunocytochemistry

Cells were seeded onto acid-washed, poly-L-lysine coated glass coverslips in 12-well plates. At midconfluency, cells were then treated as indicated for 24 hours, washed with TBS, and extracted with Brinkley Buffer 1980 for 30 seconds. Cells were fixed for 20 minutes in 4% formaldehyde, 10 mmol/L MES pH 6.1, 138 mmol/L KCl, 3 mmol/L $MgCl_2$, 2 mmol/L EGTA, 0.32 mol/L sucrose. After fixation, cells were washed with TBS and then blocked in TBS-T (0.1% Triton-X) + 2% BSA + 22.52 mg/mL glycine for 30 minutes, followed by an overnight incubation in primary antibody (Abcam179513, 1:1000) at 4°C and then secondary antibody for 1 hour at room temperature (Life Technologies, A11012, 1:500). Cells were counterstained with DAPI before mounting. Confocal imaging was performed using an A1 laser scanning confocal attachment on an Eclipse Ti microscope stand using a 60×/1.49 ApoTIRF oil-immersion objective and standard lasers and filter sets (Nikon Instruments).

Animal breeding and genotyping

Genetically engineered models were generated by intercrossing strains as listed in Supplementary Methods, with genotyping performed by Transnetyx. Strains were of mixed genetic background. Studies utilized both male and female animals. Animals were provided standard chow and housed under a 12-hour light/dark cycle.

Capan1 xenograft intervention study

Seven-week-old NCr *nu/nu* athymic nude mice were inoculated subcutaneously with 5×10^6 Capan-1 cells suspended in Matrigel ($N = 10$/group). When the mean tumor volume was approximately 212 mm^3, mice were randomized to treatment with: vehicle, PTC596 [12.5 mg/kg, twice per week (b.i.w.), orally], gemcitabine (100 mg/kg, b.i.w., i.p.), or full-dose combination of PTC596 + gemcitabine. At day 45, dosing was stopped. Length (L) and width (W) diameters of tumors were measured using digital calipers and mice were weighed twice per week. Tumor volume was calculated as $(L \times W^2)/2$.

PDX model intervention study

Study was performed by Champions Oncology. Early-passage tumor fragments from Champions model CTG-1462 were implanted subcutaneously in *nu/nu* mice and then randomized to a treatment arm once tumors reached 150–300 mm^3. Mice ($n = 5$/group) were treated on one of seven arms: vehicle, gemcitabine [50 mg/kg, once per week (q.w.), i.p.], nab-paclitaxel (10 mg/kg, i.v., q.w.×3), PTC596 (12.5 mg/kg, b.i.w.×4, p.o.), or full-dose combinations of the agents. Endpoints were when a tumor reached 1,500 mm^3 or after 90 days on study. Length (L) and width (W) diameters of tumors were measured using digital calipers and mice were weighed twice per week. Tumor volume was calculated as $(L \times W^2)/2$.

KPC intervention/survival study

Tumor formation in KPC mice was monitored by weekly palpation until the detection of a mass. Upon positive palpation, the mass was monitored by twice weekly ultrasound (15) until the tumor reached an enrollment size of 4–7 mm average diameter. After enrollment, KPC mice were randomized to vehicle, PTC596 (17 mg/kg, orally, b.i.w.), gemcitabine alone (100 mg/kg, i.p., b.i.w.), or PTC596 + gemcitabine.

Measurement of PTC596 levels in plasma and tissue samples

Concentrations of PTC596 in samples were quantified using high-performance LC/MS-MS.

Survival data synergy analysis

To test for synergy between gemcitabine and 596 treatments in the KPC intervention study, we generated a regression model for logarithm-transformed survival times from mice treated with vehicle, gemcitabine, PTC596, and an interaction term for gemcitabine + PTC596. The significance of the gemcitabine:PTC596 interaction term tests the single-tailed deviation of the combination arm from the additive effects of each agent alone.

IHC

Immunohistochemistry (IHC) was performed according to standard protocols. Slides were blocked for 1 hour at room temperature in TBS-T (0.1% Tween20) + 1.5% normal horse serum (Vector Laboratories, S-2000) + 2% Animal Free Blocker (Vector Laboratories, SP-5030). Primary antibodies were diluted in blocking solution and incubated overnight at 4°C at the indicated concentrations and then developed using the ImmPRESS and ImmPACT Kits (Vector Laboratories). PH3 (#9701, 1:100) and CC3 (#9664S, 1:100) were from Cell Signaling Technology;.

Results

PTC596 induces mitotic arrest and apoptosis in PDA cell lines

On the basis of our initial interest in the potential role of BMI1 in pancreatic cancer (16), we assessed the effects of PTC596 on the viability of PDA cell lines. We treated three human PDA lines (Aspc1, Mia PaCa-2, and Panc1) with PTC596 or vehicle and found that the agent potently reduced cell viability over the course of 96 hours in all cell lines (Fig. 1A; Supplementary Fig. S2A). The cytotoxicity of PTC596 was confirmed in colony formation assays on the same lines (Supplementary Fig. S2B). Next, we performed cell-cycle analysis using intracellular 7-AAD staining and found that PTC596 induced a G_2–M arrest, similar to the antimitotic agent nocodazole (Fig. 1B and C; Supplementary Fig. S2C). Flow cytometry for the M-phase marker phospho-histone H3 (PH3) demonstrated an accumulation of PDA cells specifically in mitosis following PTC596 treatment (Fig. 1D and E; Supplementary Fig. S2D). These data demonstrate that PTC596 acts as a potent inducer of mitotic arrest in multiple PDA cell lines.

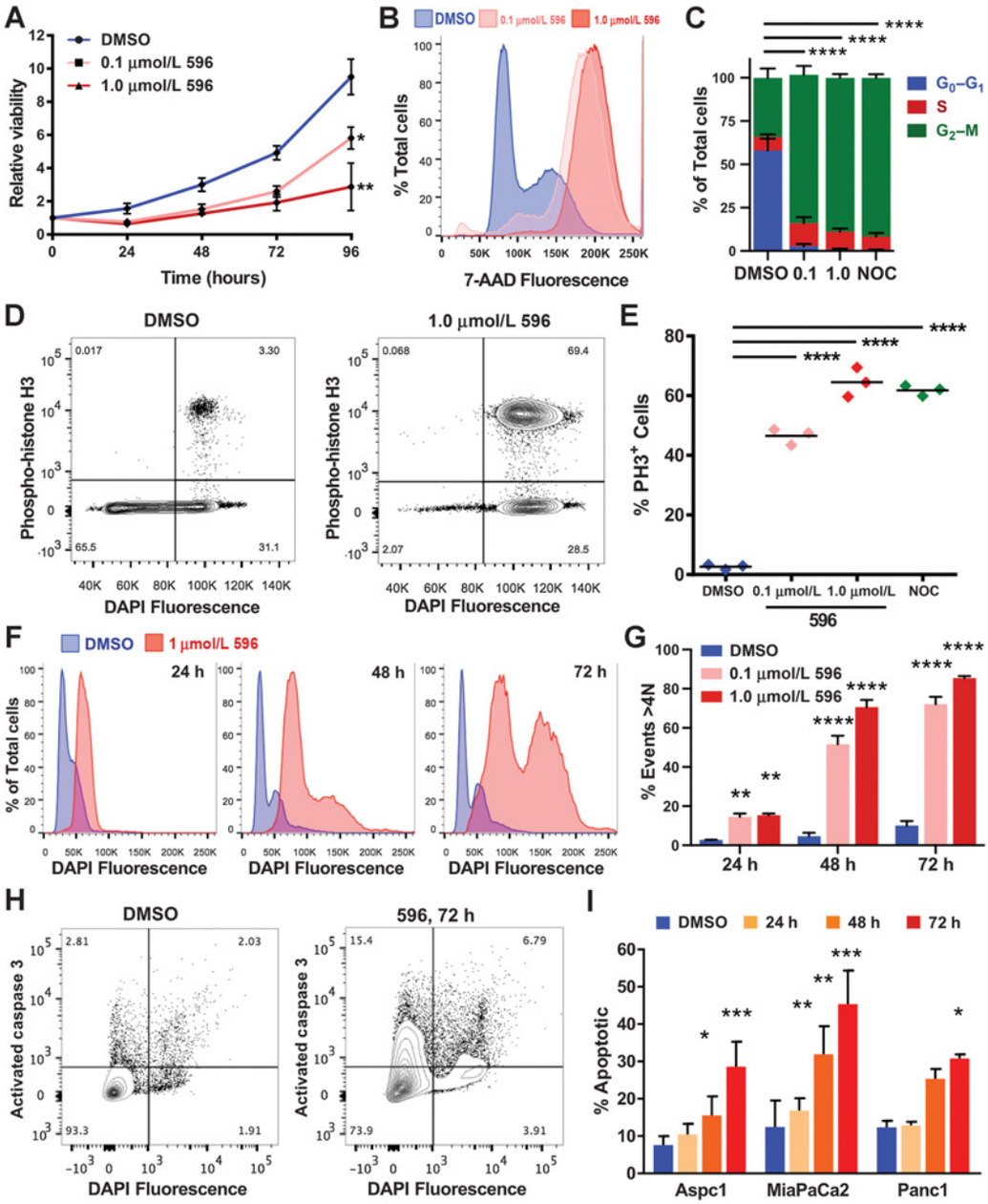

Figure 1.

PTC596 inhibits proliferation of PDA cell lines by inducing G_2–M arrest, polyploidy, and ultimately cell death. **A,** Relative Aspc1 cell viability over 96 hours following treatment with vehicle or indicated concentrations of PTC596. Asterisks indicate significance at final timepoint. **B,** Representative histograms of DNA content, measured by flow cytometry for 7-AAD fluorescence, from Aspc1 cells treated for 24 hours with vehicle or PTC596. **C,** Percent of Aspc1 cells in G_0–G_1 phase, S-phase, and G_2–M phase following 24 hours treatment with vehicle (DMSO), PTC596 (0.1 μmol/L, 1.0 μmol/L), 0.1 μmol/L nocodazole (NOC, positive control). χ^2 test with multiple hypothesis correction for indicated comparisons, with *P* values integrated across the three experiments by Stouffer method. **D,** Representative flow cytometry scatter plots of phosphorylated histone H3 (PH3) expression versus DNA content (DAPI) in Aspc1 cells treated with vehicle or PTC596 for 24 hours. **E,** Percent of Aspc1 cells in mitosis ($PH3^+$/4N DNA content) after treatment for 24 hours with DMSO, PTC596, or 0.1 μmol/L nocodazole (NOC). **F,** Representative histograms of DNA content measured by DAPI fluorescence in Aspc1 cells treated with vehicle or PTC596 at the indicated timepoints. **G,** Percent of Aspc1 cells with DNA content >4N after treatment with DMSO or PTC596 at indicated timepoints. Two-way ANOVA, paired by experiment, with Dunnett multiple comparisons test for treatment groups compared with control within each timepoint. **H,** Representative flow cytometry scatter plots showing induction of apoptosis in Aspc1 cells following treatment with DMSO for 24 hours, or 1.0 μmol/L PTC596 at 24, 48, and 72 hours. Unfixed cells were stained for active caspase-3 and DAPI to distinguish viable cells (bottom left) from early apoptosis (top left), late apoptosis (top right), and necrosis (bottom right). **I,** Total apoptotic Aspc1 cells (active caspase 3^+) were quantified for DMSO or PTC596 at each timepoint. Unless otherwise noted, statistical comparisons used a one-way ANOVA, paired by experiment, with Dunnett correction for multiple comparisons for treatment groups compared with control. Error bars depict SEM over $n = 3$ biological replicates in each experiment (*, $P < 0.05$; **, $P < 0.005$; ***, $P < 0.001$; ****, $P < 0.0001$).

The mitotic checkpoint exists to ensure that chromosomes are appropriately attached to microtubules prior to cell division (17). If the triggering stress is not resolved, prolonged mitotic arrest may result in apoptosis or, alternatively, progression into a pseudo-G_1 phase in the absence of cytokinesis. Particularly, in the context of *p53* mutations, this can lead to cell-cycle reentry and eventual polyploidization through the process of endoreduplication (18, 19). As *p53* is mutated in approximately 78% of human ductal adenocarcinomas (20), we examined DNA content in three *p53*-mutant human PDA lines following treatment with PTC596. Over the course of 72 hours, we observed a progressive increase in DNA content, eventually leading to >60% of cells bearing >4N DNA content (Fig. 1F and G; Supplementary Fig. S3A and S3B). This was accompanied by increased levels of apoptosis that progressively increased over the same timeframe in all three lines, as measured by the caspase-activated probe FITC-DEVD-FMK (Fig. 1H and I). Thus, PTC596 induces responses in pancreatic tumor cell lines consistent with prolonged mitotic checkpoint activation, including polyploidization and cell death.

PTC596 has favorable pharmacologic properties

Many candidate anticancer agents demonstrate promising activity *in vitro*, but are either too toxic or have poor pharmacologic properties when administered *in vivo*–problems that are compounded by the characteristic hypoperfusion of ductal pancreatic tumors (4). Prior work in xenograft models of acute myeloid leukemia (AML) suggested that PTC596 is generally well tolerated (21), but its delivery to solid tumor tissues has not been assessed. In anticipation of studies in the KPC model, we treated 5 PC mice per timepoint ($p53^{LSL.R172H/+}$; $Pdx1Cre^{tg/+}$ – KPC littermates that are phenotypically normal) with a single oral dose of 10 mg/kg PTC596 and examined circulating drug levels over a period of 48 hours (Fig. 2A). After 7 hours, plasma concentrations of PTC596 peaked at 8.9 μg/mL and then diminished over the course of 2 days, yielding a terminal half-life of approximately 15 hours, which compares favorably with the pharmacokinetics of other traditional cytotoxic agents. Thus, PTC596 persists in circulation for sufficient time to potentially equilibrate within poorly perfused pancreatic tumors.

In addition to imposing biophysical constraints on drug delivery, tumor cells can actively pump out many chemotherapeutic drugs via the multidrug transporter P-glycoprotein (P-gp). We examined the impact of P-gp expression and inhibition on drug sensitivity by using a congenic pair of cell lines (MDCK-WT and MDCK-PGP) with or without overexpression of human *ABCB1* (the gene encoding P-gp) and cotreating with the P-gp inhibitor Valspodar. We measured the viability of these cell lines over 72 hours in response to increasing concentrations of PTC596 or other agents, in the presence or absence of Valspodar (Fig. 2B and C). For several chemotherapeutic agents known to be P-gp substrates, including vinblastine and paclitaxel, overexpression of P-gp increased the CC_{50} by 10–30 fold, an effect that was fully reversed by cotreatment with Valspodar. In contrast, both PTC596 and its analogue PTC028 (22) were fully unaffected by P-gp overexpression or inhibition, indicating that these agents are not susceptible to this multidrug resistance mechanism.

To directly assess the delivery and accumulation of PTC596 to pancreatic tumor tissues, we performed a short-term study in pancreatic tumor-bearing KPC mice following administration of a single dose of 17 mg/kg PTC596. After 24 hours, tissues were harvested, frozen, extracted, and analyzed by mass spectrometry (Fig. 2D). Prior studies have shown that pancreatic tumor stroma limits the accumulation of other chemotherapeutic agents relative to normal tissues (4, 23). In contradistinction, PTC596 was effectively delivered to pancreatic tumor tissues, achieving levels comparable with those observed in quadriceps muscle, spleen, and brain tissues. Higher levels were detected in liver and kidney tissues, the primary routes of clearance for PTC596. We next examined whether cotreatment with gemcitabine altered the delivery of PTC596 to tissues, using a similar study design in the related $KP^{fl/fl}C$ ($Kras^{LSL.G12D}/+$; $p53^{fl/fl}$; $Pdx1\text{-}Cre^{tg/+}$) model, and found no effect of gemcitabine on the pharmacology of PTC596 (Fig. 2E). Together, these data demonstrate that PTC596 can be effectively distributed into PDA tissues, alone and in combination with gemcitabine, despite the unique biophysical constraints on drug delivery to pancreatic tumors.

Having established the effective delivery of PTC596 to tumor tissues, we next examined the pharmacodynamic response of murine pancreatic tumors to PTC596. We began by confirming that PDA cells derived from the KPC model behave similarly to human PDA cells in response to treatment with PTC596 (Supplementary Fig. S4). We then evaluated the impact of PTC596 on mitotic arrest *in vivo* by measuring expression of the mitotic protein Cyclin B1 in tumors from $KP^{fl/fl}C$ mice. We performed a second short-term intervention study in tumor-bearing $KP^{fl/fl}C$ mice ($n = 3$), this time acquiring a pretreatment biopsy by abdominal laparotomy (24) and then treating with 10 mg/kg PTC596 on days 0, 2, 4. On day 5, the mice were euthanized and tissues harvested, 24 hours after the final dose (Supplementary Fig. S5A). Western blotting for Cyclin B1 was performed on lysates from paired pre- and posttreated tumor samples (Fig. 2F). Cyclin B1 protein levels were significantly increased in posttreatment samples relative to pretreatment samples, indicating that the delivery of PTC596 to tumor tissues was sufficient to induce a pharmacodynamic response *in vivo*.

Finally, we assessed the tolerability of prolonged treatment with PTC596 in combination with gemcitabine, using KC mice ($Kras^{LSL.G12D/+}$; $Pdx1\text{-}Cre^{tg/+}$) as surrogates for the KPC model. We found that these mice tolerated up to 17 mg/kg PTC596 (orally, q.w.) in combination with 100 mg/kg gemcitabine (i.p., b.i.w) for at least 1 month (Fig. 2G). Together, these data demonstrate that PTC596 is a well-tolerated agent with a prolonged half-life and effective biodistribution that induces an acute pharmacodynamic response in pancreatic tumor tissues.

PTC596 + gemcitabine exhibit activity in preclinical models of pancreatic cancer

To begin to assess the preclinical efficacy of PTC596, we generated cell line–based xenografts from Capan-1 human PDA cells implanted subcutaneously in nu/nu mice. One week after implantation, when the implanted tumors had reached approximately 200 mm^3, mice were randomized to one of four treatment arms: vehicle, PTC596 alone at a submaximal dose for this strain (12.5 mg/kg, b.i.w., orally), gemcitabine (40 mg/kg, b.i.w., i.p.), or both agents combined ($N = 10$/group). Over the course of 45 days, we found that PTC596 slowed tumor growth modestly as a monotherapy (Fig. 3A), and induced transient regressions in combination with gemcitabine. Both regimens were well tolerated as evidenced by longitudinal weight measurements (Fig. 3B).

Next, to evaluate the activity of PTC596 in a more physiologically accurate model, we carried out an intervention/survival study in the KPC genetically engineered mouse model. Nascent

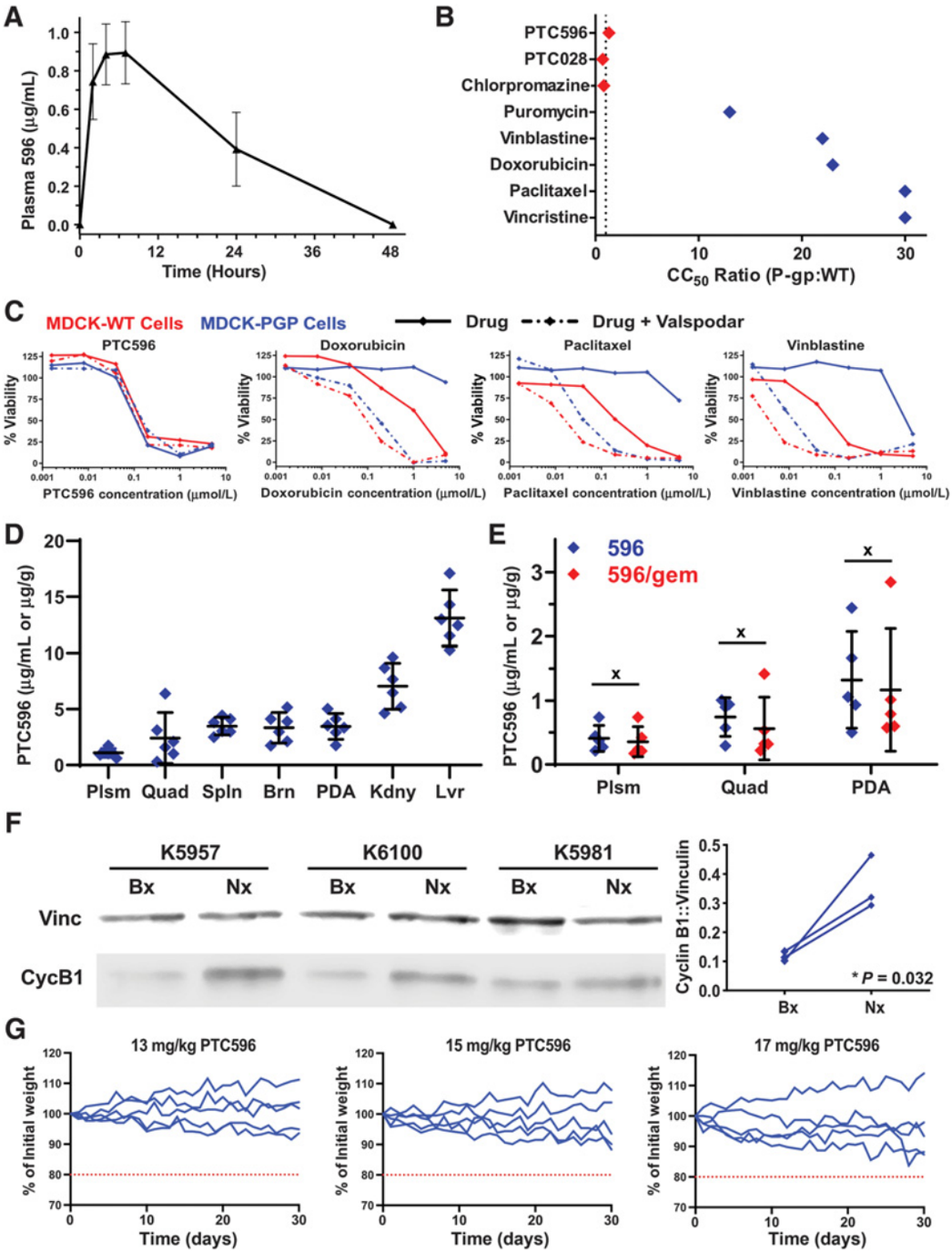

Figure 2.

PTC596 has properties favorable for *in vivo* administration. **A,** Plasma levels of PTC596 as measured by mass spectrometry at baseline, or 2, 4, 7, 24, or 48 hours follwing a single oral dose of PTC596 (10 mg/kg). Error bars, SD. $n = 5$ mice per time point. **B,** Ratio of CC_{50} values for PTC596 treatment of MDCK-P-gp versus MDCK-WT cells. **C,** Viability dose–response curves of the indicated drugs for MDCK-WT (red) and MDCK-P-gp (blue) cells, alone (solid lines) or cotreated with the P-gp inhibitor Valspodar (dashed lines). **D,** Mass spectrometry measurements of PTC596 concentrations in tumor and normal tissues from six KPC, 24 hours following a single oral dose of PTC596 (17 mg/kg). **E,** PTC596 concentrations in plasma (Plsm), quadriceps (Quad), and PDA tissues from $KP^{f/f}C$ mice, 24 hours post a single oral dose of PTC596 (10 mg/kg), alone or in combination with gemcitabine (100 mg/kg). **F,** Left, Western blot analysis for CYCLIN B1 on tumors from $KP^{fl/fl}C$ mice treated with 10 mg/kg PTC596 alone ($n = 3$). Tumor biopsy samples (Bx) were acquired by abdominal laparotomy 48 hours prior to first dose, and compared with samples acquired at necropsy (Nx) 24 hours after the third dose. Right, quantification of CYCLIN B1 (CycB1) from the left, normalized to VINCULIN (Vinc). *, $P < 0.05$ by paired *t* test. **G,** Body weights of KC mice treated for 30 days with PTC596 (q.w., orally) in combination with gemcitabine (100 mg/kg, b.i.w., i.p.). PTC596 was administered at 13 mg/kg, 15 mg/kg, or 17 mg/kg. Brn, brain; Kdny, kidney; Lvr, liver; Spln, spleen.

autochthonous pancreatic tumors were identified and measured by high-resolution 3D ultrasound (15) and the volume of each tumor was tracked longitudinally during treatment (Supplementary Fig. S5B). Mice were randomized to one of four treatment arms: vehicle, PTC596 alone (17 mg/kg, b.i.w., orally), gemcitabine (100 mg/kg, b.i.w., i.p.), or PTC596 + gemcitabine (full-dose combination); this regimen was well-tolerated in tumor-bearing KPC mice (Fig. 3C). Strikingly, while neither PTC596 nor gemci-

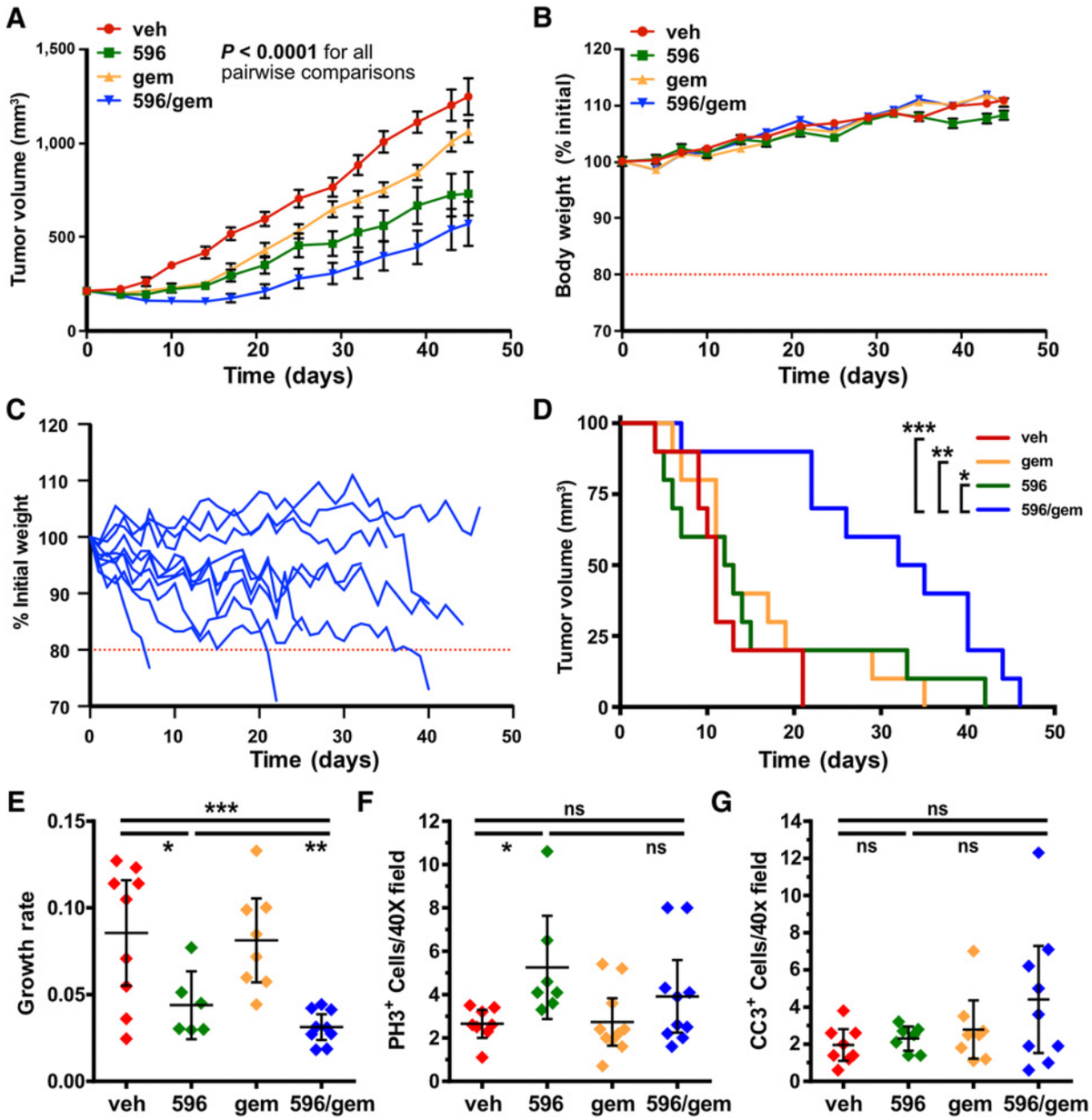

Figure 3.

Combinatorial efficacy of PTC596 with gemcitabine in preclinical models of PDA. **A,** nu/nu mice bearing Capan-1 xenograft tumors were treated with vehicle, PTC596 (12.5 mg/kg, b.i.w.), gemcitabine (40 mg/kg, b.i.w.), or PTC596 + gemcitabine for 45 days. Tumor volumes were measured twice per week. Bars, SD. $N = 10$ mice per treatment group. **B,** Body weights from mice in **A** are plotted as percent original body weight. Bars, SD. **C,** Body weights of KPC mice treated with 596/gemcitabine shows the regimen is well tolerated until mice succumb to disease. **D,** Survival of KPC mice treated with vehicle (veh), gemcitabine (gem, 100 mg/kg, b.i.w.), PTC596 (596, 17 mg/kg, b.i.w.), or PTC596 + gemcitabine (596/gem). Median overall survival of the 596/gemcitabine arm was 33.5 days versus 11, 12.5, and 12.5 for the remaining arms. $N = 10$ mice/treatment arm. Significant pairwise comparisons indicated (log-rank test). **E,** Tumor growth rates calculated from longitudinal tumor volumes. Statistical comparisons show one-way ANOVA with Sidak correction for the indicated pairs. **F,** Quantification of IHC for phosphorylated Histone H3 (PH3) performed on KPC intervention study tumors following necropsy. Plots show average positive cells per 40× field over 10 fields per tumor. Bars, SEM. One-way ANOVA with Sidak correction. **G,** Quantification of IHC for cleaved caspase-3 (CC3) performed on KPC intervention study tumors following necropsy. Plots show average positive cells per 40× field over 10 fields per tumor. Bars, SEM. One-way ANOVA with Sidak correction (*, $P < 0.05$; **, $P < 0.005$; ***, $P < 0.001$; ****, $P < 0.0001$).

tabine alone impacted survival, we found that the two agents synergistically increased overall survival by more than 3-fold over vehicle-treated animals ($P = 0.033$ for interaction term of a Cox proportional hazards model; Fig. 3D). Using longitudinal 3D ultrasound data, we reconstructed growth curves for each tumor over time and found that while PTC596 + gemcitabine did not induce tumor regressions, the combination durably reduced tumor growth rate (Supplementary Fig. S5C and S5D). Using a published algorithm (25), we modeled the growth/decay kinetics of each tumor and found that PTC596 reduced tumor growth rate both in combination with gemcitabine, and also as a monotherapy (Fig. 3E; Supplementary Fig. S5E). Examination of liver sections revealed no significant difference in the fraction of animals free of metastasis following treatment (Supplementary Fig. S5F).

We next assessed whether PTC596 induced mitotic arrest in the KPC tumors using IHC for phospho-Histone H3 (PH3). We found that PH3 was significantly elevated in the PTC596 monotherapy group compared with vehicle (Fig. 3F), consistent with an increased mitotic fraction (Supplementary Fig. S6A–S6D). A trend toward increased PH3 staining was also observed in the combination treated mice; we speculate that the induction of G_1 arrest by gemcitabine reduces the fraction of cells arrested in mitosis, consistent with the overall lower growth rate of tumors treated with PTC596 + gemcitabine.

Finally, we performed IHC for the apoptotic marker cleaved caspase-3 (CC3) on the same endpoint tumor samples. While none of the treatments significantly elevated the overall fraction of CC3-positive cells (Fig. 3G), half of the tumors in the PTC596/gemcitabine group exhibited elevated levels of apoptosis relative to vehicle-treated tumors (Supplementary Fig. S6E and S6F). This finding is notable given that the samples were collected at endpoint when the tumors have largely escaped the initial effects of drug treatment. Together, these findings demonstrate that PTC596 can contribute to an effective anticancer response in models of PDA, particularly as part of a combination regimen with a standard-of-care agent.

PTC596 functions independent of *Bmi1* in PDA cells

PTC596 was previously reported to be a BMI1 inhibitor (21). However, the induction of mitotic arrest by PTC596 in multiple cell lines (Fig. 1) contrasts with the findings of several prior studies in which silencing of *Bmi1* with shRNAs or miRNAs was shown to induce a G_1 arrest (26–30). In both human PDA and AML (21) cell lines, PTC596 treatment was associated with hyperphosphorylation of BMI1 (Fig. 4A and B), suggesting the possibility that modulation of BMI1 is a component of the mechanism of action of PTC596. Incidentally, we noted that nocodazole, a chemical that induces mitotic arrest through inhibition of tubulin polymerization, also induces BMI1 hyperphosphorylation (Fig. 4A). Indeed, BMI1 was previously reported to be phosphorylated and dissociated from chromatin during mitosis, indicating that BMI1 phosphorylation is cell-cycle–dependent (31). Thus, PTC596 may impact BMI1 as an indirect consequence of inducing mitotic arrest; however, the functional role of BMI1 in the activity of PTC596 is uncertain.

To directly assess the role of Bmi1 in PTC596 activity, we used a dual recombinase strategy to generate *Kras*$^{FSF.G12D}$/+; *Tp53*$^{R172H/+}$; *Pdx1-FlpO*$^{tg/+}$; *Bmi1*$^{fl/fl}$; *Rosa26*$^{CreERT2/+}$ (KPFBR) mice, in which the *Bmi1* gene can be acutely deleted in the context of *Kras/p53*–mutant pancreatic tumors (see Materials and Methods). We derived a PDA cell line (J1002) from an autochthonous pancreatic tumor arising in a KPFBR mouse, and treated it *in vitro* with 4-hydroxy-tamoxifen or vehicle, yielding congenic lines that were wild-type (J1002VEH) or null (J1002TAM) for *Bmi1* (Fig. 4C and D). We then treated each line with PTC596 and examined cell viability over the course of 96 hours. Notably, *Bmi1* deletion in J1002 cells did not impact the ability of PTC596 to inhibit cell proliferation (Fig. 4E and F) or induce mitotic arrest (Fig. 4G and H). These studies indicate that the antiproliferative effects of PTC596 in pancreatic tumor cells are not dependent on the function of BMI1.

PTC596 inhibits microtubule polymerization

To learn more about the impact of PTC596 on PDA cells, we performed RNA sequencing on Aspc1 cells treated with either DMSO or 1.0 μmol/L PTC596 for 8, 16, and 24 hours. Integrating the data from experimental and control samples across all three timepoints, we found that genes differentially expressed between PTC596 versus DMSO-treated cells were strongly enriched in mitotic processes and depleted in processes associated with S-phase or the G_1–S transition (Supplementary Fig. S7A). Moreover, PTC596 treatment led to significant downregulation of multiple α- and β-tubulin genes (Fig. 5A). Indeed, tubulin genes accounted for 8 of 10 of the most downregulated genes in response to PTC596 treatment. Tubulin gene transcripts are subject to tight autoregulation based on the abundance of free tubulin monomer, which increases following inhibition of tubulin polymerization (32). These findings led us to hypothesize that PTC596 might function as a microtubule polymerization inhibitor.

We first tested this hypothesis through ultracentrifugation of protein lysates from vehicle or PTC596-treated Aspc-1, Mia PaCa-2, and Panc1 cells. In this assay, large polymerized microtubules pellet at low speeds (5,000 × *g*), whereas free tubulin monomers remain in the supernatant even following high-speed ultracentrifugation (100,000 × *g*). Visualization of tubulin fractions by Western blotting demonstrated that PTC596 treatment led to a near-complete loss of polymerized microtubules, similar to the effects of colchicine, a well-known microtubule polymerization inhibitor (Fig. 5B; Supplementary Fig. S7B). Consistent with this finding, we observed a striking loss of polymerized microtubules in three different human PDA lines following PTC596 treatment, as visualized by β-tubulin immunofluorescence, with the few remaining microtubules assuming an altered, irregular pattern (Fig. 5C and D; Supplementary Fig. S7C).

Microtubule polymerization is facilitated and regulated by numerous cellular proteins (33). To determine whether PTC596 directly affects microtubule polymerization, we carried out a biochemical polymerization assay using >99% purified tubulin and GTP in a reaction buffer. We assessed the impact of PTC596 in this cell-free assay at multiple concentrations. Notably, we found that PTC596 inhibited tubulin polymerization in a dose-dependent manner, similar to colchicine, whereas paclitaxel, a microtubule-stabilizing agent, accelerated polymerization kinetics (Fig. 5E and F). These findings demonstrate that PTC596 functions as a direct inhibitor of microtubule polymerization.

The preclinical efficacy of PTC596 in PDA is synergistic with gemcitabine/nab-paclitaxel

PTC596 and nab-paclitaxel appear to share several similarities. Both are MTAs with attractive pharmacologic properties and both combine effectively with gemcitabine in the treatment of PDA, at

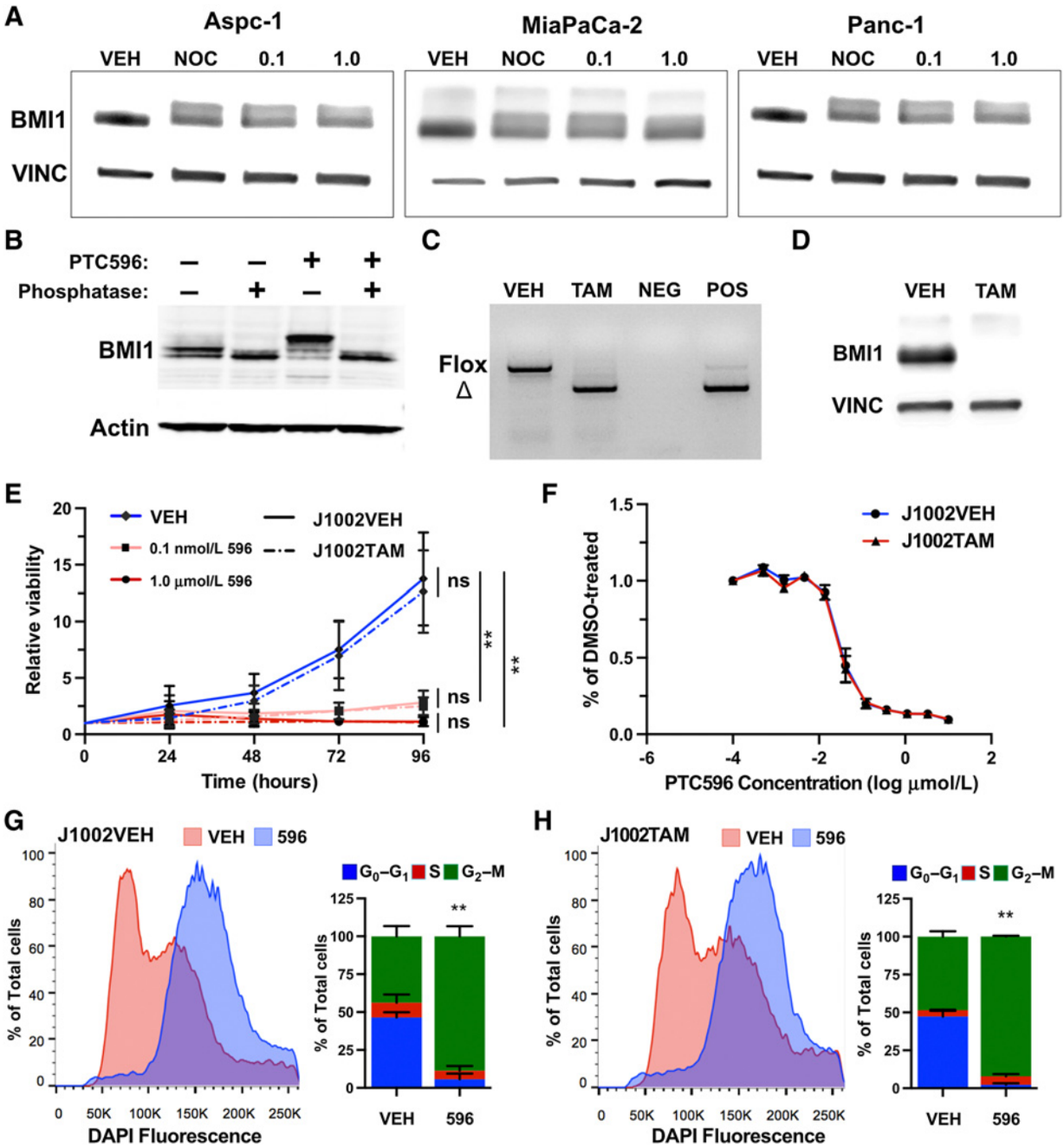

Figure 4.

The activity of PTC596 is independent of BMI1 in PDA cells. **A,** Western blots showing BMI1 levels in Aspc1, MiaPaCa-2, and Panc1 cells treated for 24 hours with vehicle (VEH), 0.1 μmol/L nocodazole (NOC), 0.1 μmol/L 596 (0.1), or 1.0 μmol/L 596 (1.0) relative to Vinculin (VINC) loading control. Both PTC596 and nocodazole induce accumulation of a lower mobility band. **B,** Treatment of HT1080 protein lysates with λ phosphatase demonstrates that the lower mobility band induced by PTC596 is due to phosphorylation. **C,** PCR showing *Bmi1* deletion in J1002 cells following treatment with tamoxifen. Top band represents floxed allele. Bottom band represents recombined allele after treatment. VEH, cells treated with 0.02% ethanol for 72 hours; TAM, cells treated with 5 μmol/L tamoxifen for 72 hours; NEG, no DNA. POS, DNA from kidney tissue of a KPFBR mouse treated with tamoxifen. **D,** Western blot showing loss of BMI1 protein expression in J1002TAM cells. **E,** Relative viability of J1002VEH and J1002TAM cells treated with vehicle, 0.1 μmol/L 596, or 1.0 μmol/L 596 over 96 hours. Bars, SEM, $N = 3$ biological replicates, one-way ANOVA with Dunnett correction comparing treatment groups with VEH. **F,** Dose–response curves for J1002VEH and J1002TAM cells treated with PTC596 for 72 hours. Viable cells quantified at endpoint by AlamarBlue. Bars, SEM, $N = 3$ biological replicates. DNA content flow cytometry for J1002VEH cells (**G**) and J1002TAM cells (**H**). Left, Representative DNA histograms for cells treated for 24 hours with vehicle (VEH) or 1.0 μmol/L PTC596. Right, Percent of cells in G_0–G_1 phase, S-phase, G_2–M phase for cells treated for 24 hours with vehicle (VEH) or 1.0 μmol/L PTC596 (596). Bars, SEM, $N = 3$ biological replicates, *t* test with Welch correction. For all panels, *, $P < 0.05$; **, $P < 0.005$; ***, $P < 0.001$; ****, $P < 0.0001$.

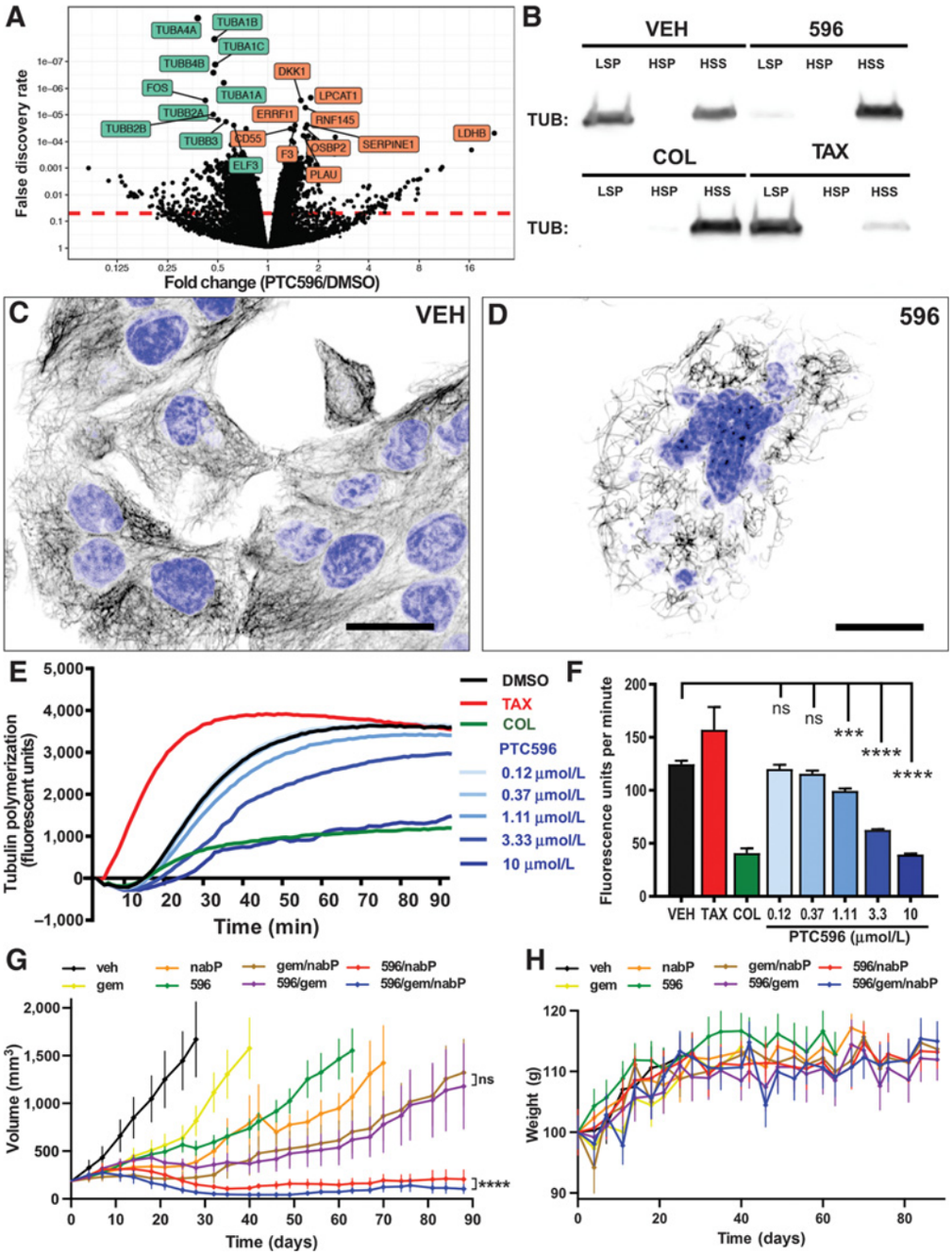

Figure 5.

PTC596 directly inhibits tubulin polymerization and synergizes with nab-paclitaxel *in vivo*. **A,** Plot of differentially expressed genes measured by RNA-seq on ASPC1 cells treated with DMSO or 1 μmol/L PTC596, integrated over 8, 16, and 24 hour timepoints. Subsets of downregulated (green) and upregulated (orange) genes in cells treated with PTC596 are indicated. **B,** Representative Western blot analysis from Aspc1 cells treated with vehicle (VEH), 3.0 μmol/L PTC596 (596), 1.0 μmol/L colchicine (COL), or 1.0 μmol/L paclitaxel (TAX) for 2 hours. After treatment, cell lysates were fractionated by centrifugation to separate free tubulin from microtubules. LSP, low speed pellet (1,000 × *g*, 5 minutes); HSP, high speed pellet (100,000 × *g*, 1 hour); HSS, high speed supernatant (100,000 × *g*, 1 hour). Representative immunofluorescence images of Aspc1 cells treated with vehicle (**C**) or PTC596 (**D**) for 24 hours. β-Tubulin is shown in black and DAPI in blue. $N = 3$ biological replicates. Scale bar, 20 μm. **E,** Cell-free tubulin polymerization assay showing the ability of PTC596 to directly inhibit polymerization of free tubulin. **F,** Maximal slope (fluorescence units/minute = polymerization rate) of three independent replicates of experiment in **E** shows that PTC596 significantly decreased the polymerization rate of tubulin, similar to colchicine (COL) and opposite of paclitaxel (TAX). Bars, SEM, one-way ANOVA with Dunnett correction for treatment groups compared with VEH. ***, $P < 0.001$; ****, $P < 0.0001$. **G,** Average tumor volumes over time of subcutaneous patient-derived xenografts derived from a human PDA for the indicated treatment groups. Bars, SEM, $N = 5$ tumors per group. Selected two-way ANOVA comparisons indicated (ns, not significant; ****, $P < 0.0001$). **H,** Percent of initial body weight over time for the mice from **G**.

least in a preclinical setting. However, nab-paclitaxel is already clinically approved in combination with gemcitabine for the treatment of metastatic PDA, and now serves as a prominent backbone regimen for clinical trials of new investigational agents. Given this clinical landscape, is there a rationale for adding a microtubule polymerization inhibitor to a regimen that already includes a microtubule-stabilizing agent?

Combinations of multiple MTAs have been explored clinically in several cancers, particularly in breast cancer where the combination of vinorelbine + paclitaxel was found to be tolerable and have promising efficacy in a phase II trial of second-line patients with advanced disease (34). However, multi-MTA regimens have not been explored in the context of PDA. We therefore carried out a 7-arm intervention study using a PDA patient-derived xenograft model, evaluating all combinations of gemcitabine, nab-paclitaxel, and PTC596 ($n = 5$ per arm). As expected, pairing gemcitabine with nab-paclitaxel slowed tumor growth to a greater degree than either agent alone (Fig. 5G), and this was reflected in growth constants derived from their respective tumor volume curves (Supplementary Fig. S7D). In this model, PTC596 exhibited similar anticancer activity to nab-paclitaxel, both as a monotherapy and in combination with gemcitabine. Strikingly, the triple combination of gemcitabine/nab-paclitaxel/gemcitabine had a remarkable effect on the viability of this PDX model, producing sizeable and durable regressions in all 5 animals evaluated, including one complete response (Supplementary Fig. S7E and S7F). The induction of tumor regressions was evident in our modeling of tumor volume kinetics, which produced a decay term for all 5 animals, 3 of which had no associated growth term. Moreover, the increased efficacy of this regimen was achieved without a measurable impact on tolerability, as evidenced by longitudinal weight measurements (Fig. 5H). Unexpectedly, we noted that the two-drug combination of nab-paclitaxel + PTC596 was nearly as active as the three-drug combination, yielding regressions in 4 of 5 tumors. Thus, rather than functioning through redundant mechanisms, we found that the combination of a microtubule polymerization inhibitor with a microtubule stabilizer yielded a potent synergistic effect on preclinical efficacy in PDA without appreciable effects on tolerability.

Discussion

Over the course of 65 years, MTAs have been the most successful class of anticancer agents, with approved applications in leukemia, lymphoma, breast, non–small cell lung, and pancreatic cancers, among others. First approved by the FDA in 1962 (35), vincristine (Oncovin) was initially isolated from the periwinkle plant (*Catharanthus roseus*) and determined to be myeloablative, with anticancer activity in models of lymphocytic leukemia (36). Over the subsequent decades, more than half a dozen additional MTAs received FDA approval, mostly for oncology applications. Different subclasses of these agents are distinguished by their binding sites on tubulin, which determines their ability to inhibit or stabilize microtubule polymerization. However, as a class, MTAs have been limited by broad toxicities, poor pharmacologic properties, and an overly simplistic understanding of the cellular mechanism(s) through which they induce antineoplastic activity. In the past few decades, two major advances were made with the FDA approvals of eribulin (Halavan) and nab-paclitaxel (Abraxane), with each proving informative as to how further advances may be realized.

Prior to the development of eribulin, all clinical MTAs bound to one of three sites on tubulin: the vinca and colchicine sites for inhibitors of microtubule polymerization and the taxane site for microtubule stabilizers. In contrast, eribulin inhibits microtubule polymerization through noncompetitive binding to another site, resulting in the formation of small globular aggregates of tubulin (rather than releasing free tubulin, like prior polymerization inhibitors) (37). This subtle mechanistic difference is associated with reduced toxicity relative to vinca agents and has led to approvals in metastatic breast cancer and liposarcoma (38). Given that colchicine, eribulin, vinca agents, and taxanes all effectively reduce the normal function of tubulin and induce mitotic arrest, why might their activity and toxicity profiles vary so broadly?

As microtubules play a critical role in the separation of chromosomes during mitosis, resulting in mitotic arrest, it was long assumed that the primary antineoplastic mechanism of MTAs was through mitotic checkpoint activation. On the basis of this logic, inhibitors of several mitotic checkpoint proteins, including aurora kinases, polo-like kinases, and kinesin spindle protein, were developed (39–41). However, across 46 clinical trials for 20 mitosis–specific inhibitors, the overall response rate was just 1.6% (42). Therefore, the most relevant antineoplastic effects of MTAs may, in fact, be their impact on other microtubule-associated processes. Indeed, one of the main side effects of MTAs as a class is neurotoxicity, which is mediated by effects on postmitotic neurons. Microtubule dynamics play critical roles in the functioning of HSPs, endosomal trafficking, cell migration, and other key aspects of cell biology (43–45). Similarly, some MTAs induce vascular remodeling in addition to tumor cell apoptosis, through uncertain mechanisms (46, 47). These cellular functions are mediated by distinct pools of microtubules with different biochemical properties conferred by interactions with varying sets of microtubule-associated proteins. Thus, subtle differences in the binding of an MTA to tubulin will likely have diverse impacts on various cellular functions.

The second recently approved MTA was nab-paclitaxel, a reformulated variant of the microtubule-stabilizing agent paclitaxel. The key advance of nab-paclitaxel is its improved pharmacology over native paclitaxel, which is poorly soluble and rapidly cleared from circulation. A carrier agent, Cremophor, is utilized for solubilization of paclitaxel in the clinical formulation, but Cremophor itself confers significant additional toxicity. In nab-paclitaxel, the parent drug is stabilized by binding to albumin, increasing its solubility while lowering toxicity and maintaining prolonged stability in circulation. Given that drug delivery is compromised in PDA due to poor perfusion and diffusion within the tumor parenchyma (4), prolonged circulation and low toxicity are desirable features for novel agents against this disease. Indeed, in 2015, a positive phase III trial of nab-paclitaxel in combination with gemcitabine led to its approval for use in metastatic pancreatic cancer (7).

Together, these examples proffer a compelling case that novel MTAs have the potential to play an important role in the future of oncology, particularly those with novel biochemistry, attractive pharmacology, and low toxicity. PTC596 provides a strong example of such an agent, with a long circulating half-life and evidence of the accumulation of efficacious concentrations of the agent in genetically engineered pancreatic tumors. It is worth noting that tubulin is among the most abundant proteins in a proliferating cell, and thus may act as a sink for the stabilization and retention of tubulin-binding drugs. Combined with the lack of drug efflux

via P-glycoprotein, these features may serve to elevate intratumoral concentrations while limiting peripheral toxicity. Indeed, in a multicenter phase I study in advanced solid tumors (NCT02404480), PTC596 was generally well tolerated through six dose levels and target plasma concentrations were achieved well below the highest dose (48). Primary side effects were manageable and generally gastrointestinal in nature. Critically, no evidence of peripheral neuropathy was observed, distinguishing PTC596 from nearly all other MTAs. A phase Ib study in combination with paclitaxel and carboplatin for patients with advanced ovarian cancer (NCT03206645) is ongoing.

Both in ovarian cancer and in PDA, current backbone regimens include taxanes, raising the question of whether adding a microtubule polymerization inhibitor is likely to confer additional benefit. The principle rationale for combining such agents is that they may each impact different subsets of microtubule functions in different ways. Preclinical synergy between vinca agents and taxanes has been reported both *in vitro* (49, 50) and *in vivo* (51) and multiple early-phase clinical trials have been performed in breast, non–small cell lung, and other cancers (34). For example, in a clinical study of paclitaxel and vinorelbine in metastatic breast cancer, 6 complete responses and 19 partial responses were observed among 52 patients. While main toxicities were neutropenia and neurotoxicity, they were reported to be mild and well tolerated (52). Thus, there is both rationale and precedent for combining microtubule polymerization inhibitors and stabilizers in an oncology setting. In that context, the observation of durable regressions in a pancreatic cancer PDX model exclusively among tumors treated with both nab-paclitaxel and PTC596 is a highly promising signal of preclinical efficacy. Ideally, this combination would have also been evaluated in an autochthonous model system such as KPC mice; however, the human albumin component of nab-paclitaxel induces anaphylaxis in immune-competent animals after prolonged exposure (53, 54). Nonetheless, even the two-drug combination of PTC596 + gemcitabine produced a 3-fold extension of overall survival in the KPC model, matching or exceeding the best responses reported to date for this highly chemoresistant model. Taken together, we believe these data provide strong rationale for the clinical development of PTC596 combination strategies in the context of pancreatic ductal adenocarcinoma.

Disclosure of Potential Conflicts of Interest

A. Branstrom is an employee of and holds ownership interest (including patents) in PTC Therapeutics. K.P. Olive reports receiving commercial research grants from PTC Therapeutics. No potential conflicts of interest were disclosed by the other authors.

Authors' Contributions

Conception and design: J.A. Eberle-Singh, L. Cao, M. Weetall, K.P. Olive
Development of methodology: L. Cao, M. Weetall, K.P. Olive
Acquisition of data (provided animals, acquired and managed patients, provided facilities, etc.): J.A. Eberle-Singh, I. Sagalovskiy, S.A. Sastra, C.F. Palermo, A.R. Decker, A. Mollin, A. Branstrom, M. Weetall, K.P. Olive
Analysis and interpretation of data (e.g., statistical analysis, biostatistics, computational analysis): J.A. Eberle-Singh, I. Sagalovskiy, H.C. Maurer, A.R. Decker, L. Cao, J. Hu, M. Weetall, K.P. Olive
Writing, review, and/or revision of the manuscript: J.A. Eberle-Singh, I. Sagalovskiy, H.C. Maurer, A.R. Decker, J. Hu, A. Branstrom, M. Weetall, K.P. Olive
Administrative, technical, or material support (i.e., reporting or organizing data, constructing databases): M.J. Kim, J. Sheedy, A. Mollin, A. Branstrom
Study supervision: L. Cao, M. Weetall, K.P. Olive

Acknowledgments

K.P. Olive received support for this work from the NCI (1R21CA188857), the Stewart Trust Cancer Research Fellowship, and sponsored research support from PTC Therapeutics. J.A. Eberle-Singh received support from an NIH training grant (5T32CA009503). The *Bmi1*^{flox} allele was generously provided by the laboratory of Dr. Marina Pasca di Magliano, with permission from Dr. Sean Morrison, who generated the allele. The Pdx-FlpO allele was kindly provided by E. Scott Seeley. The work made use of several shared resources of the Herbert Irving Comprehensive Cancer Center (P30CA013696) including: Confocal and Specialized Microscopy, Flow Cytometry, Small Animal Imaging, and Molecular Pathology.

The costs of publication of this article were defrayed in part by the payment of page charges. This article must therefore be hereby marked *advertisement* in accordance with 18 U.S.C. Section 1734 solely to indicate this fact.

Received October 5, 2018; revised March 26, 2019; accepted June 3, 2019; published first June 7, 2019.

References

1. Raimondi S, Maisonneuve P, Lowenfels AB. Epidemiology of pancreatic cancer: an overview. Nat Rev Gastroenterol Hepatol 2009;6:699–708.
2. Siegel RL, Miller KD, Jemal A. Cancer statistics, 2019. CA Cancer J Clin 2019;69:7–34.
3. Howlader N, Noone AM, Krapcho M, Miller D, Brest A, Yu M, et al. SEER Cancer Statistics Review, 1975–2014. Available from: https://seer.cancer.gov/csr/1975_2014/.
4. Olive KP, Jacobetz MA, Davidson CJ, Gopinathan A, McIntyre D, Honess D, et al. Inhibition of Hedgehog signaling enhances delivery of chemotherapy in a mouse model of pancreatic cancer. Science 2009;324:1457–61.
5. Neesse A, Algul H, Tuveson DA, Gress TM. Stromal biology and therapy in pancreatic cancer: a changing paradigm. Gut 2015;64:1476–84.
6. Hingorani SR, Petricoin EF, Maitra A, Rajapakse V, King C, Jacobetz MA, et al. Preinvasive and invasive ductal pancreatic cancer and its early detection in the mouse. Cancer Cell 2003;4:437–50.
7. Von Hoff DD, Ervin T, Arena FP, Chiorean EG, Infante J, Malcolm Moore M, et al. Increased survival in pancreatic cancer with nab-paclitaxel plus gemcitabine. N Engl J Med 2013;369:1691–703.
8. Joerger M. Metabolism of the taxanes including nab-paclitaxel. Expert Opin Drug Metab Toxicol 2015;11:691–702.
9. Kim MJ, Cao L, Sheedy J, Risher N, Dumble M, Lee CS, et al. PTC596-induced Bmi1 hyper-phosphorylation via Cdk1/2 activation resulting in tumor stem cell depletion [abstract]. In: Proceedings of the 105th Annual Meeting of the American Association for Cancer Research; 2014 Apr 5-9; San Diego, CA. Philadelphia (PA): AACR; 2014. Abstract nr 5517.
10. Dobin A, Davis CA, Schlesinger F, Drenkow J, Zaleski C, Jha S, et al. STAR: Ultrafast Universal RNA-Seq Aligner. Bioinformatics 2013;29:15–21.
11. Lawrence M, Huber W, Pages H, Aboyoun P, Carlson M, Gentleman R, et al. Software for computing and annotating genomic ranges. PLoS Comput Biol 2013;9:e1003118.
12. Carlson M, Maintainer BP. TxDb.Hsapiens.UCSC.hg19.knownGene: Annotation Package for TxDb Object(s); 2015. https://bioconductor.org/packages/release/data/annotation/html/TxDb.Hsapiens.UCSC.hg19.knownGene.html.
13. Ritchie ME, Phipson B, Wu D, Hu Y, Law CW, Shi W, et al. Limma powers differential expression analyses for RNA-sequencing and microarray studies. Nucleic Acids Res 2015;43:e47.
14. Hanzelmann S, Castelo R, Guinney J. GSVA: gene set variation analysis for microarray and RNA-seq data. BMC Bioinformatics 2013;14:7.
15. Sastra SA, Olive KP. Quantification of murine pancreatic tumors by high-resolution ultrasound. Methods Mol Biol 2013;980:249–66.

16. Bednar F, Schofield HK, Collins MA, Yan W, Zhang Y, Shyam N, et al. . Bmi1 is required for the initiation of pancreatic cancer through an Ink4a-independent mechanism. Carcinogenesis 2015;36:730–8. doi 10.1093/carcin/bgv058.
17. Vleugel M, Hoogendoorn E, Snel B, Kops GJ. Evolution and function of the mitotic checkpoint. Dev Cell 2012;23:239–50.
18. Leonardo AD, Khan SH, Linke SP, Greco V, Seidita G, Wahl GM. DNA rereplication in the presence of mitotic spindle inhibitors in human and mouse fibroblasts lacking either p53 or pRb function. Cancer Res 1997;57:1013–9.
19. Xu WS, Perez G, Ngo L, Handrick R, Wahl C, Leptihn S, et al. Induction of polyploidy by histone deacetylase inhibitor: a pathway for antitumor effects. Cancer Res 2005;65:7832–9.
20. Waddell N, Pajic M, Patch AM, Chang DK, Kassahn KS, Bailey P, et al. Whole genomes redefine the mutational landscape of pancreatic cancer. Nature 2015;518:495–501.
21. Nishida Y, Maeda A, Kim MJ, Cao L, Kubota Y, Ishizawa J, et al. The novel BMI-1 inhibitor PTC596 downregulates MCL-1 and induces p53-independent mitochondrial apoptosis in acute myeloid leukemia progenitor cells. Blood Cancer J 2017;7:e527.
22. Dey A, Xiong X, Crim A, Dwivedi SKD, Mustafi SB, Mukherjee P, et al. Evaluating the mechanism and therapeutic potential of PTC-028, a novel inhibitor of BMI-1 function in ovarian cancer. Mol Cancer Ther 2018;17:39–49.
23. Provenzano PP, Cuevas C, Chang AE, Goel VK, Von Hoff DD, Hingorani SR. Enzymatic targeting of the stroma ablates physical barriers to treatment of pancreatic ductal adenocarcinoma. Cancer Cell 2012;21:418–29.
24. Sastra SA, Olive KP. Acquisition of mouse tumor biopsies through abdominal laparotomy. Cold Spring Harb Protoc 2014;2014:47–56.
25. Wilkerson J, Abdallah K, Hugh-Jones C, Curt G, Rothenberg M, Simantov R, et al. Estimation of tumour regression and growth rates during treatment in patients with advanced prostate cancer: a retrospective analysis. Lancet Oncol 2017;18:143–54.
26. Jacobs JJL, Kieboom K, Marino S, DePinho RA, van Lohuizen M. The oncogene and Polycomb group gene bmi-1 regulates cell proliferation and senescence through the ink4a locus. Nature 1999;397:164–8.
27. Song W, Tao K, Li H, Jin C, Song Z, Li J, et al. Bmi-1 is related to proliferation, survival and poor prognosis in pancreatic cancer. Cancer Sci 2010;101:1754–60.
28. Wu SQ, Niu WY, Li YP, Huang HB, Zhan R. miR-203 inhibits cell growth and regulates G1/S transition by targeting Bmi-1 in myeloma cells. Mol Med Rep 2016;14:4795–801.
29. Wang L, Liu JL, Yu L, Liu XX, Wu HM, Lei FY, et al. Downregulated miR-495 [corrected] inhibits the G1-S phase transition by targeting Bmi-1 in breast cancer. Medicine 2015;94:e718.
30. Zheng X, Wang Y, Liu B, Liu C, Liu D, Zhu J, et al. Bmi-1-shRNA inhibits the proliferation of lung adenocarcinoma cells by blocking the G1/S phase through decreasing cyclin D1 and increasing p21/p27 levels. Nucleic Acid Ther 2014;24:210–6.
31. Voncken JW, Schweizer D, Aagaard L, Sattler L, Jantsch MF, van Lohuizen M. Chromatin-association of the Polycomb group protein BMI1 is cell cycle-regulated and correlates with its phosphorylation status. J Cell Sci 1999;112:4627–39.
32. Cleveland DW, Lopata MA, Sherline P, Kirschner MW. Unpolymerized tubulin modulates the level of tubulin mRNAs. Cell 1981;25:537–46.
33. Goodson HV, Jonasson EM. Microtubules and microtubule-associated proteins. Cold Spring Harb Perspect Biol 2018;10:1–20.
34. Spano JP, Bouillet T, Boaziz C, Piperno-Neumann S, Brunel P, Hennebelle F, et al. Phase II study of paclitaxel combined with vinorelbine in patients with advanced breast cancer. Am J Clin Oncol 2004;27:317–21.
35. Costa G, Hreshchyshyn MM, Holland JF. Initial clinical studies with vincristine. Cancer Chemother Rep 1962;24:39–44.
36. Bates D, Eastman A. Microtubule destabilising agents: far more than just antimitotic anticancer drugs. Br J Clin Pharmacol 2017;83:255–68.
37. Jordan MA, Kamath K, Manna T, Okouneva T, Miller HP, Davis C, et al. The primary antimitotic mechanism of action of the synthetic halichondrin E7389 is suppression of microtubule growth. Mol Cancer Ther 2005;4:1086–95.
38. Seetharam M, Kolla KR, Chawla SP. Eribulin therapy for the treatment of patients with advanced soft tissue sarcoma. Future Oncol 2018;14:1531–45.
39. Garland LL, Taylor C, Pilkington DL, Cohen JL, Von Hoff DD. A phase I pharmacokinetic study of HMN-214, a novel oral stilbene derivative with polo-like kinase-1-interacting properties, in patients with advanced solid tumors. Clin Cancer Res 2006;12:5182–9.
40. LoRusso PM, Goncalves PH, Casetta L, Carter JA, Litwiler K, Roseberry D, et al. First-in-human phase 1 study of filanesib (ARRY-520), a kinesin spindle protein inhibitor, in patients with advanced solid tumors. Invest New Drugs 2015;33:440–9.
41. Cheung CH, Coumar MS, Hsieh HP, Chang JY. Aurora kinase inhibitors in preclinical and clinical testing. Expert Opin Investg Drugs 2009;18:379–98.
42. Komlodi-Pasztor E, Sackett DL, Fojo AT. Inhibitors targeting mitosis: tales of how great drugs against a promising target were brought down by a flawed rationale. Clin Cancer Res 2012;18:51–63.
43. Kulkarni RP, Castelino K, Majumdar A, Fraser SE. Intracellular transport dynamics of endosomes containing DNA polyplexes along the microtubule network. Biophys J 2006;90:L42–4.
44. Ganguly A, Yang H, Sharma R, Patel KD, Cabral F. The role of microtubules and their dynamics in cell migration. J Biol Chem 2012;287:43359–69.
45. Giustiniani J, Daire V, Cantaloube I, Durand G, Poüs C, Perdiz D, et al. Tubulin acetylation favors Hsp90 recruitment to microtubules and stimulates the signaling function of the Hsp90 clients Akt/PKB and p53. Cell Signal 2009;21:529–39.
46. Schwartz EL. Antivascular actions of microtubule-binding drugs. Clin Cancer Res 2009;15:2594–601.
47. Kanthou C, Tozer GM. Microtubule depolymerizing vascular disrupting agents: novel therapeutic agents for oncology and other pathologies. Int J Exp Pathol 2009;90:284–94.
48. Infante JR, Bedard PL, Shapiro G, Bauer TM, Prawira A, Laskin O, et al. Phase I results of PTC596, a novel small molecular targeting cancer stem cells (CSCs) by reducing levels of BMI1 protein. J Clin Oncol 2017;35:2574–4.
49. Photiou A, Shah P, Leong LK, Moss J, Retsas S. *In vitro* synergy of paclitaxel (taxol) and vinorelbine (navelbine) against human melanoma cell lines. Eur J Cancer 1997;33:463–70.
50. Giannakakou P, Villalba L, Li H, Poruchynsky M, Fojo T. Combinations of pacliataxel and vinblastine and their effects on tublin polymerization and cellular cytotoxicity: Characterization of a synergistic schedule. Int J Cancer 1998;75:57–63.
51. Knick VC, Eberwein DJ, Miller CG. Vinorelbine tartrate and paclitaxel combinations- enhanced activity against *in vivo* P388 murine leukemia cells. J Natl Cancer Inst 1995;87:1072–7.
52. Martin M, Lluch A, Casado A, Carbonero IG, de Paz L, Esteban C, et al. Paclitaxel plus vinorelbine- An active regimen in metastatic breast cancer patients with prior anthracycline exposure. Ann Oncol 2000;11:85–9.
53. Frese KK, Neesse A, Cook N, Bapiro TE, Lolkema MP, Jodrell DI, et al. nab-Paclitaxel potentiates gemcitabine activity by reducing cytidine deaminase levels in a mouse model of pancreatic cancer. Cancer Discov 2012;2:260–9.
54. Neesse A, Frese KK, Chan DS, Bapiro TE, Howat WJ, Richards FM, et al. SPARC independent drug delivery and antitumour effects of nab-paclitaxel in genetically engineered mice. Gut 2014;63:974–83.